Nano Research

Open Access

Research Article

Structurally tunable polytetrafluoroethylene nanofiber membranes derived by *in-situ* fibrillation technology with polycaprolactone as precursor for high-performance filtration and separation applications

Zilai Wang[1,2], Guilong Wang[1,2] ✉, Jialong Chai[1,2], Runze Shao[1,2], and Guoqun Zhao[1,2]

[1] *State Key Laboratory of Advanced Equipment and Technology for Metal Forming, Shandong University, Jinan 250061, China*
[2] *Key Laboratory for Liquid-Solid Structural Evolution and Processing of Materials (Ministry of Education), Shandong University, Jinan 250061, China*

Cite this article: *Nano Research*, **2026**, *19*, 94908740. https://doi.org/10.26599/NR.2026.94908740

ABSTRACT: Porous polytetrafluoroethylene (PTFE) membranes are widely used in high-efficiency filtration, protective ventilation, and medical applications, but their traditional stretching-based preparation methods suffer from significant problems such as pollution, high energy consumption, and lengthy processes. Here, we prepared PTFE nanofiber membranes based on *in-situ* fiber forming technology. Exploiting the excellent melt processability of polycaprolactone (PCL) over a wide temperature window (90–180 °C), a microstructure-controllable fabrication strategy for PTFE nanofiber membranes was developed. By systematically regulating processing temperature, screw speed, and circulation time, the shear force imposed on PTFE crystals was precisely tuned, enabling fine control over fiber diameter, pore size, and membrane thickness. The resulting PTFE nanofiber membranes exhibit tunable fiber diameters (70–185 nm), pore sizes (0.23–1.4 μm), and thicknesses (8–24 μm), while maintaining a high porosity (> 76%). The membranes demonstrate excellent tensile strength of up to 25.3 MPa and outstanding chemical stability. In oil–water separation, the membranes show high oil permeance and separation efficiency. Moreover, in high-precision solid–liquid filtration, the membranes achieve a rejection rate approaching 99.9% for submicron particles such as carbon nanotubes (CNTs), significantly outperforming commercial stretched PTFE membranes in filtration precision. This research provides a versatile strategy with high structural customizability to address the challenges in controlled fabrication of PTFE nanofiber membranes and their application in high-precision filtration fields.

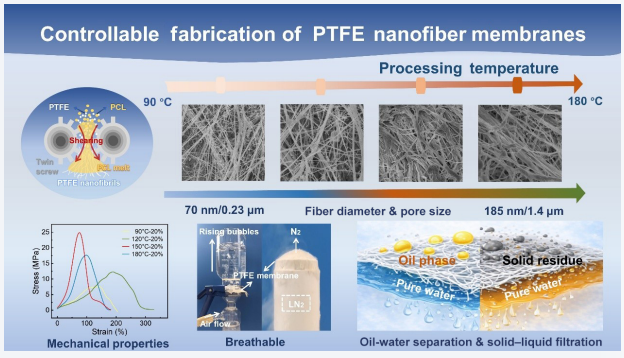

KEYWORDS: polytetrafluoroethylene (PTFE), nanofiber membrane, *in-situ* fibrillation, wide temperature processing, microstructure regulation, filtration precision

1 Introduction

In the field of modern industry including semiconductor manufacturing, biopharmaceuticals, and hydrometallurgy, the production processes continuously generate oily wastewater along with submicron solid particulate contaminants (e.g., silica in polishing slurries, carbon nanotubes (CNTs) in catalysts, and metal powders in wastewater). These pollutants not only compromise product purity but also lead to severe environmental pollution [1–4]. According to recent industry reports and market analyses, wastewater management and treatment generated during manufacturing processes (such as those in the semiconductor and other high-precision industries) has become a persistently growing and non-negligible key operational cost. Data indicates that the global wastewater treatment market related solely to the semiconductor sector has already reached a scale of tens of billions of US dollars, clearly demonstrating the increasingly profound economic impact of this aspect on the industry [5]. Traditional separation technologies such as distillation [6, 7], centrifugation

Received: February 9, 2026; **Revised:** April 13, 2026
Accepted: April 16, 2026

✉Address correspondence to guilong@sdu.edu.cn

[8–11], and flotation [12, 13], though applied in certain fields, generally suffer from issues like high energy consumption, low efficiency, and difficulty in handling micro-nanoscale particles [14–16]. Especially when dealing with emulsified oils and submicron particles, these conventional methods often fail to meet the separation accuracy required by modern industries [17, 18].

Membrane separation technology is increasingly adopted because of its attractive benefits, including no need for phase change, ease of operation, compact design, cost efficiency, and low energy consumption. However, its core challenge lies in balancing high separation accuracy with large processing flux while maintaining stable performance in harsh chemical environments [2, 19–23]. Microporous membranes composed of nanofibers are highly preferred due to their large specific surface area, high porosity, and adjustable pore size distribution [24–27]. Nevertheless, most polymer nanofiber membranes prepared via techniques such as electrospinning exhibit poor solvent resistance, making it difficult to ensure long-term stable operation under harsh conditions involving strong acids, strong bases, or organic solvents [28–30].

Polytetrafluoroethylene (PTFE) is considered an excellent material for fabricating high-performance filtration membranes because of its exceptional thermal stability, chemical inertness, and inherently low surface energy [31–33]. However, the non-melt-processable and insoluble nature of PTFE makes it incompatible with traditional technologies such as electrospinning, and it cannot be processed into nanofiber structures using conventional melt-spinning or solution-spinning techniques [34]. Currently, the stretching method is the mainstream industrial technique for producing PTFE microporous membranes. Yet, this method fails to maintain membrane uniformity and cannot achieve a balance among high porosity, fine pore size and consistent pore size distribution. Moreover, the presence of abundant "node-fibril" structures within the membrane limits its separation accuracy and flux [35, 36]. In addition, advanced techniques such as reagent-assisted porosity [37, 38], emulsion spinning [39, 40], laser ablation [41], and three-dimensional (3D) printing [42, 43] have been used to produce microporous PTFE films, but achieving films with high porosity, fine pore size, thin thickness, and strong mechanical properties remains a challenge.

In-situ fibrillation technology provides a novel approach to address this challenge, enabling the structural and controllable fabrication of microporous membranes with high porosity and ultrafine pores. This technique disperses PTFE within a processable polymer matrix. Due to the unique fibrillation behavior of PTFE crystals, shear forces applied by the screw during melt blending induce the fibrillation of PTFE. Subsequently, the polymer matrix is removed via solvent washing, yielding a PTFE nanofiber network structure. Previous studies (e.g., by Chai et al.) predominantly utilized polylactic acid (PLA) as the matrix [44, 45]. However, the relatively narrow processing window of PLA (typically above 170 °C) limits, to some extent, the capability to precisely control the morphology of PTFE nanofibers over a broader range.

Polycaprolactone (PCL) as the matrix is a biodegradable polyester characterized by a low melting point (~ 60 °C) and an exceptionally wide processing temperature range (stable processing can be achieved as low as 90 °C). This unique advantage enables this research to comprehensively explore the impact of processing temperature on the *in-situ* fibrillation of PTFE across a broad temperature span from 90 to 180 °C. At lower temperatures, the higher melt viscosity of PCL can exert stronger shear forces on PTFE, facilitating the formation of fine, uniform, and densely entangled nanofiber networks, which lays the foundation for achieving high-precision filtration. Conversely, at higher temperatures, the reduced viscosity leads to weaker shear forces, resulting in the tendency to form coarser and more loosely structured fibers. This exceptional tunability based on a wide temperature range allows for the "customized" fabrication of PTFE nanofiber membranes with specific pore sizes and fiber structures to meet varying filtration accuracy and flux requirements. Furthermore, the nanofibers produced using PCL as the matrix are finer, which is more advantageous for application scenarios such as filtration. This study proposes an environmentally friendly, simple, and low-cost strategy for structurally tunable fibrillation. It focuses on simulating the solid–liquid and oil–water separation performance of this series of membranes under harsh environmental conditions, particularly their retention accuracy for submicron particles. This demonstrates their promising application potential in high-end filtration fields.

2 Experiments

2.1 Materials

Polytetrafluoroethylene (METABLEN-A3800) was sourced from Mitsubishi Chemical Co., Japan. Polycaprolactone (CAPA™ 6800) with a density of 1.16 g/cm^3 and a melt flow rate (MFR) of 7.3 g/10 min (measured at 190 °C/2.16 kg) was supplied by Perstorp Group, Sweden. Dichloromethane (CH_2Cl_2) and chloroform ($CHCl_3$) were procured from China National Pharmaceutical Chemical Co., Ltd.

2.2 Preparation of PTFE nanofiber membranes

During the pretreatment phase, PTFE and PCL pellets were subjected to vacuum drying at 50 °C for 12 h to eliminate any residual moisture. After weighing, the dried PTFE/PCL blends (with PTFE mass fractions of 10%, 20%, and 30%) were introduced into a mini twin-screw extruder (SJZS-10B, Ruiming, Wuhan, China). The melt processing was conducted for 10 min at temperatures of 90, 120, 150, and 180 °C. The initial residence time was set to 5 min, with variations in screw speed and cycle times to meet experimental requirements. Afterward, the extruded material was hot-pressed into circular films with a thickness of 90 μm at 100 °C and 10 MPa, followed by natural cooling. The obtained PTFE/PCL blend films were soaked in dichloromethane, cleaned three times, and subjected to Soxhlet extraction at 45 °C for 8 h to fully eliminate the PCL matrix, leaving the PTFE nanofiber network. Lastly, the purified PTFE nanofiber membranes were vacuum-dried at 60 °C for 24 h. The prepared membrane samples were labeled as *T*-*X*, where *T* denotes the processing temperature (°C), and *X* refers to the initial PTFE mass fraction (wt.%) in the PTFE/PCL blend.

2.3 Characterizations and measurements

Rheological properties: The rheological behavior of the PTFE/PCL melts was assessed using a rotational rheometer (Mars 40, Haake, Germany) equipped with a parallel-plate geometry, and conducted under a nitrogen atmosphere. For pure PCL, a dynamic temperature sweep was performed across a temperature range of 60–200 °C with a heating rate of 3 °C/min, a strain amplitude of 1%, and an angular frequency of 10 rad/s. For the PTFE/PCL

blends, dynamic frequency sweep tests were carried out at a strain amplitude of 1% at temperatures of 90, 120, 150, and 180 °C, and the angular frequency range was from 0.1 to 100 rad/s.

Microstructure: The morphology of fiber was examined using a scanning electron microscope (SEM, G500). The fiber diameter distribution was quantified using Image-Pro Plus software based on measurements of more than 200 fibers.

Membrane thickness and pore size: The membrane thickness was evaluated with a laser confocal microscope. The pore size distribution of the membranes was assessed using a capillary flow porometer (CFP-1500AE, PMI, USA, Beijing Best, BSD-PBL).

Porosity: Porosity is calculated using Eq. (1). The porosity (ε) of the PTFE nanofiber membranes was calculated using a gravimetric method [46] with n-butanol as the wetting liquid. It was calculated based on the amount of liquid retained within the membrane pores

$$\varepsilon = \frac{(m_1 - m_2)/\rho_1}{(m_1 - m_2)/\rho_1 + m_2/\rho_s} \quad (1)$$

where m_1 represents the wet membrane weight, m_2 represents the dry membrane weight, ρ_1 is the density of liquid (0.8097 g/mL of n-butanol), and ρ_s is the density of PTFE (2.2 g/cm^3).

Mechanical properties: The mechanical properties of the PTFE nanofiber membranes were assessed using a universal testing apparatus (MTS Exceed E43) for tensile testing (sample dimensions: 40 mm × 5 mm; tensile speed: 1 mm/min).

Air permeability: The air permeability of the PTFE nanofiber membrane samples was evaluated at room temperature and under liquid-nitrogen-cooled conditions using a Buchner funnel (500 mL) and a custom-built air permeability testing device.

Water contact angle (WCA): WCA was measured using a contact angle goniometer (JC2000D, Powereach, China) to evaluate the wettability of the PTFE nanofiber membranes.

Oil–water filtration performance: To evaluate filtration, dye-stained water and chloroform solutions were applied onto flat-sheet membranes, and both static and dynamic images were captured. The PTFE nanofiber membranes were fixed on a Buchner funnel. For mixtures without surfactants, 10 mL of oil (dyed with Sudan red) was combined with 10 mL of deionized water (dyed with methylene blue) and mixed at a 1:1 ratio (v:v). In the case of surfactant-stabilized emulsions, 1 g of Span80 was dissolved in 95 mL of oil and then mixed with 5 mL of water. The resulting mixture was stirred for 2–3 min and subjected to low-power ultrasonication for 15 min to ensure complete dissolution. The prepared oil-water emulsions were then directly poured onto the fiber membranes, with the separation driven by gravity. The liquid flux (F) is determined using Eq. (2) [47]

$$F = \frac{V}{S \times t} \quad (2)$$

where V represents the volume of permeate (L), S is the effective area of the membrane (m^2), and t refers to the permeation time (h). The separation efficiency (η_m) of oil/water mixtures is calculated using Eq. (3)

$$\eta_m = \frac{m_1}{m_2} \times 100\% \quad (3)$$

where m_2 and m_1 are the masses of oil in the oil–water mixture before and after separation, respectively. The separation efficiency of oil-in-water emulsions can be calculated using Eq. (4)

$$\eta_e = 1 - \frac{c_1}{c_2} \times 100\% \quad (4)$$

Here, c_2 and c_1 represent the water contents in 50 μL of oil before and after separation, respectively, as determined by a Karl Fischer moisture analyzer (BCS-600, Benchuang, China).

Furthermore, the cyclic usability and antifouling performance of the membranes were evaluated. After 10 consecutive separation cycles, changes in filtration flux during the process were recorded. The PTFE fiber membranes were cleaned with ethanol, and the changes in flux during 10 subsequent cycles of separation were recorded. It was compared with the membrane flux data obtained before cleaning.

Chemical stability: Membrane samples were immersed in 98% H_2SO_4 and 40% NaOH solutions for 30 min. After immersion, their structural integrity was examined using SEM to observe any potential changes.

Solid–liquid filtration performance: The flux of different fiber membranes for pure water and pure oil (chloroform) was assessed using a Buchner funnel and a vacuum filtration system under a pressure of 1.5 bar. Before testing, PTFE fiber membranes were pre-wetted with ethanol. The flux of the pure liquid was determined using Eq. (5)

$$F' = \frac{V}{S \times t \times P} \quad (5)$$

where F' is the flux of pure liquid, P is the driving pressure. Three types of suspensions were prepared to simulate pollutants under different conditions: Silica suspension: 100 mg/L of 0.5 μm SiO_2 microspheres dispersed in ethanol solution (containing 0.15% Span-80). Copper powder suspension: 200 mg/L of copper powder dispersed in deionized water (containing 0.1% Polyvinylpyrrolidone (PVP)). CNTs suspension: 50 mg/L of CNTs dispersed in dilute H_2SO_4 solution (pH = 2) (containing 0.5% sodium dodecylbenzene sulfonate (SDBS)).

Taking the CNTs dispersed in dilute sulfuric acid as an example: 50 mg of CNTs were added to 55 mL of diluted H_2SO_4 solution (5 mL of 98% H_2SO_4 + 50 mL deionized water), followed by ultrasonic dispersion for 3 h. Vacuum filtration was performed at 0.5 bar, and the CNTs retained on the filter membrane were collected, dried, and weighed. The retention rate (R%) was calculated using Eq. (6)

$$R\% = \frac{m_1}{m_2} \times 100\% \quad (6)$$

where m_2 and m_1 represent the mass of CNTs added before filtration and retained after filtration, respectively.

3 Results and discussion

3.1 Fabrication and characterization of PCL-based PTFE nanofiber membrane

As shown in Fig. 1, PTFE nanofiber membranes were fabricated via an *in-situ* fibrillation approach. Due to the unique surface properties of PTFE crystals, shear forces can be applied at a certain temperature to unwind and deform into nanofibrillated structures [48]. During processing, PTFE was thermomechanically compounded with PCL. The molten PCL acted as a transient processing medium and lubricant, enabling efficient transfer of shear stress from the rotating screw to the PTFE phase, thereby promoting PTFE disentanglement, elongation, and fibrillation.

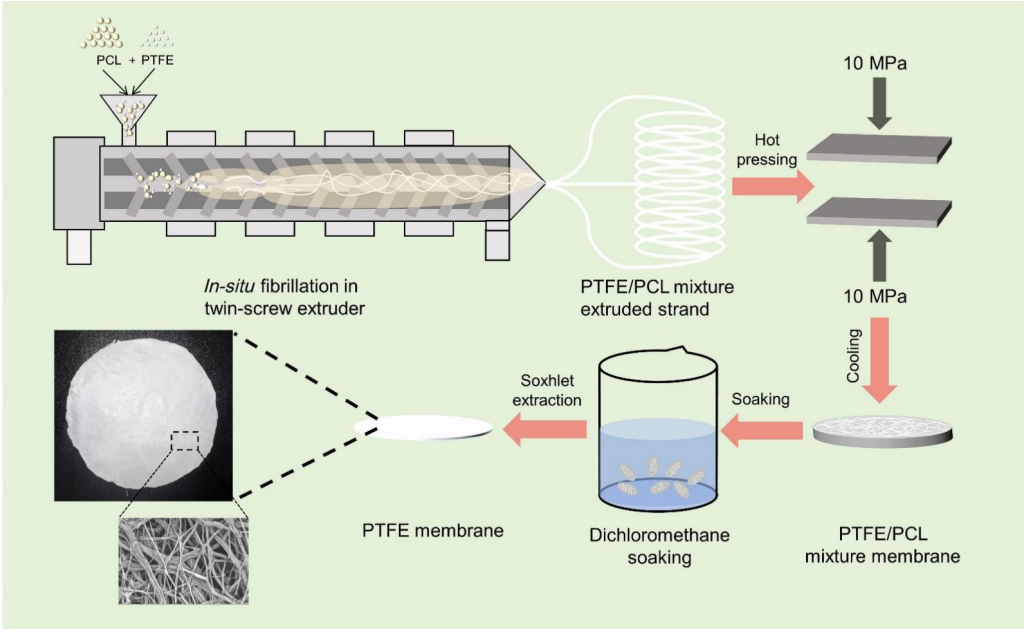

Figure 1 Schematic of preparing PTFE nanofiber membrane by *in-situ* fibrillation with PCL as precursor.

Continuous rotational shear ensured homogeneous dispersion of PTFE, followed by extensive inter-fibrillar entanglement, leading to the formation of a three-dimensional nanofibrous network. Subsequently, the PTFE/PCL blend was hot-pressed into a membrane and subjected to repeated solvent extraction to completely remove the PCL matrix, resulting in a self-supporting porous membrane composed exclusively of nanofibrillated PTFE. Notably, both the PCL and the solvent used in this process are recyclable, contributing to reduced material consumption and improved resource efficiency.

In Fig. 2(a), the schematic illustrates that the shear force from the twin-screw is transmitted to the PTFE phase indirectly via the viscous PCL melt. As the processing matrix, PCL plays a critical role in determining the degree of fibrillation of the PTFE fiber membrane. The melting point of PCL is approximately 60 °C (Fig. S1 in the Electronic Supplementary Material (ESM)). Its complex viscosity decreases gradually with increasing temperature, allowing the PTFE/PCL blend system to exhibit controllable and continuous viscosity variations over a broad temperature range of 65–200 °C (Fig. 2(b)). Accordingly, four processing temperatures (90, 120, 150, and 180 °C) were selected to apply varying shear forces to the PTFE, thereby achieving different degrees of fibrillation. The PTFE/PCL blend (20 wt.% PTFE) exhibits distinct complex viscosity (η^*) values at different temperatures (Fig. 2(c)). Two dimensionless parameters, the capillary number (Ca) and the Deborah number (De) [49, 50], are introduced to quantitatively elucidate the fibrillation process of PTFE. Ca represents the ratio of viscous forces to interfacial tension (Eq. (S1) in the ESM). When viscous forces dominate, the dispersed phase is more prone to deformation and fiber formation. De is defined as the ratio of relaxation time to characteristic process time (Eq. (S2) in the ESM). De < 1 indicates viscous fluid behavior, with a smaller De leading to easier fiber retraction. Table S1 in the ESM shows that both parameters vary with processing temperature. The degree of fibrillation correlates well with Ca and De. SEM results (Figs. 2(d)–2(g)) clearly demonstrate the significant influence of processing temperature on PTFE fiber morphology. It can be observed that PTFE membranes processed at different temperatures all display distinct nanofibrous structures, with the average fiber diameter increasing as the processing temperature rises (Table S2 in the ESM). Figure 2(h) displays the diameter distribution of PTFE fibers processed at different temperatures. At the low temperature of 90 °C, the highly viscous PCL melt exerts extremely strong shear forces on PTFE particles, inducing the formation of a fine, uniform, and highly entangled nanofiber network, with most resulting fibers being finer than 100 nm. As the processing temperature increases, the melt viscosity decreases and shear forces weaken, leading to a gradual rise in the mean diameter of the formed PTFE fibers. At 150 and 180 °C, the fiber structure becomes looser, with increased fiber diameters and significantly broader diameter distributions, where both finer (~ 100 nm) and coarser (~ 600 nm) fibers coexist. Meanwhile, variations in the processing temperature also cause variations in the pore size of the membrane. Figure 2(i) presents the pore size distribution of PTFE nanofiber membranes fabricated at various processing temperatures. Increasing the processing temperatures results in looser fiber structures and broader pore size distributions, forming more large-sized pores. With increasing processing temperature, the mean pore size expanded from 0.23 μm at 90 °C to 1.4 μm at 180 °C. Notably, PTFE nanofiber membranes prepared at various processing temperatures but with the identical PTFE content exhibit similar porosities, with all membranes maintaining a high porosity of over 76% (Fig. 2(j)). This provides a structural basis for evaluating the separation performance (oil/water, solid/liquid separation) and air permeability of the PTFE nanofiber membranes is thereby established.

Studies indicate that the initial PTFE/PCL mass ratio also influences the microstructure of PTFE nanofiber membranes. Three initial PTFE contents (10 wt.%, 20 wt.%, and 30 wt.%) were chosen to prepare PTFE nanofiber membranes at 150 °C. As illustrated in Figs. 3(a)–3(c), the nanofiber membranes prepared with different PTFE contents exhibit similar fibrillation behavior and all possess highly fibrillated structures. However, as further revealed in Figs. 3(d)–3(f), distinct differences in their

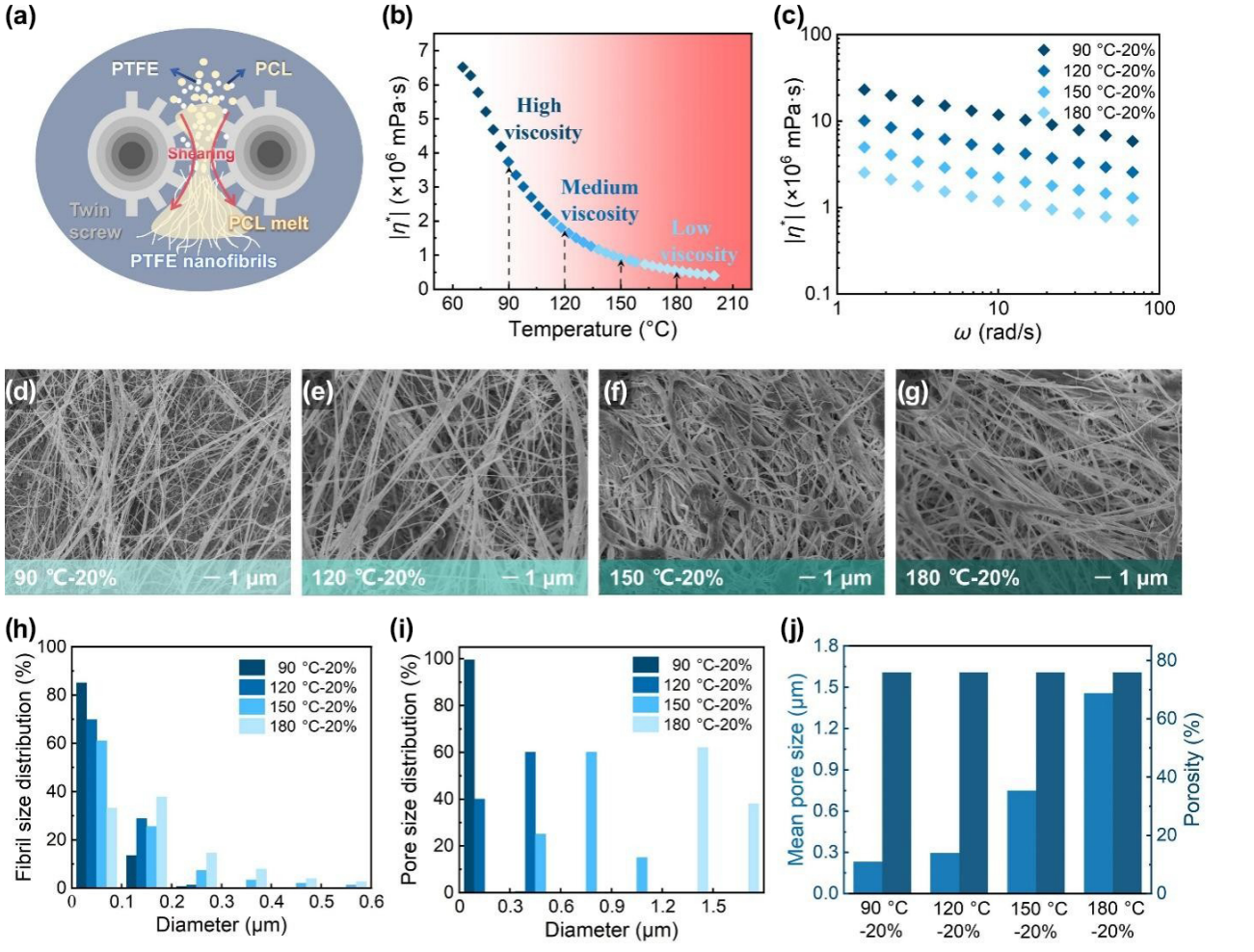

Figure 2 (a) Schematic diagram of shear force transmission in a twin-screw extruder. (b) Schematic diagram of the complex viscosity ($|\eta^*|$) of PCL under temperature scanning. (c) Frequency-dependent $|\eta^*|$ of the PTFE/PCL blend at different temperatures. Representative SEM micrographs of PTFE nanofiber membranes fabricated at (d) 90 °C, (e) 120 °C, (f) 150 °C, and (g) 180 °C. Corresponding quantitative results include (h) fibril diameter distribution, (i) pore size distribution, and (j) pore size and porosity.

microstructures can still be observed. The fiber diameters exhibit slight differences, as shown in Fig. 3(d) and Table S3 in the ESM. A higher PTFE content results in a larger fraction of finer fibers. This is because increasing the PTFE loading significantly enhances the probability of interparticle contact and phase continuity, allowing shear stress to be more efficiently transferred to the PTFE phase. This promotes the elongation and fibrillation of PTFE crystallites rather than their fragmentation, thereby increasing the proportion of finer nanofibers and leading to a more developed and interconnected fibrous network structure. As illustrated in Fig. 3(e), PTFE/PCL blends with different ratios exhibit comparable complex viscosity magnitudes ($|\eta^*|$) at the same temperature. Consequently, the three PTFE fiber membranes exhibit comparable pore size distribution profiles, mainly concentrated in the 0.7–0.9 μm range (Table S4 in the ESM). As the PTFE content increases, the mean pore size and porosity of the membranes show a slight decrease—specifically, from 0.76 to 0.74 μm and from 82% to 67%, respectively (Fig. 3(f)). This trend can be attributed to the increased fiber density. The fibrillation degree and fiber morphology of PTFE fiber membranes are primarily determined by the shear forces applied to PTFE crystals, with only a minor influence from the initial PTFE content.

This study further investigates the effect of cycle time and extruder screw speed on the morphology of PTFE nanofiber membranes. In the PCL-based *in situ* fibrillation system, the screw speed is a key parameter affecting the intensity of the shear field. To explore its influence, PTFE/PCL blends (10 wt.% PTFE) were prepared at a fixed processing temperature (150 °C) and cycle time (5 min) with different screw speeds (set to 20, 30, and 40 r/min). The differences in shear force are directly reflected in the final microstructure of the PTFE nanofiber membranes. Representative SEM images reveal that PTFE successfully formed nanofiber structures under all conditions (Figs. 3(a), 3(g), and 3(h)). The degree of fibrillation increased with the screw speed. Quantitative analysis of the fiber diameter and membrane pore size (Fig. 3(i)) quantitatively reveals this trend: As the screw speed increases, the average fiber diameter shows a slight decrease (from 0.29 to 0.22 μm), whereas the pore size changed significantly with screw speed. At lower screw speeds (20 r/min), the fibrillation of PTFE was insufficient, with the mean pore size of the fiber membrane reaching 1.2 μm. At 30 r/min, the fibers became more entangled, and the average pore size decreased to around 1 μm. At the higher screw speed of 40 r/min, the fiber network became finer and more uniform, with the mean pore size further reduced to 0.8 μm.

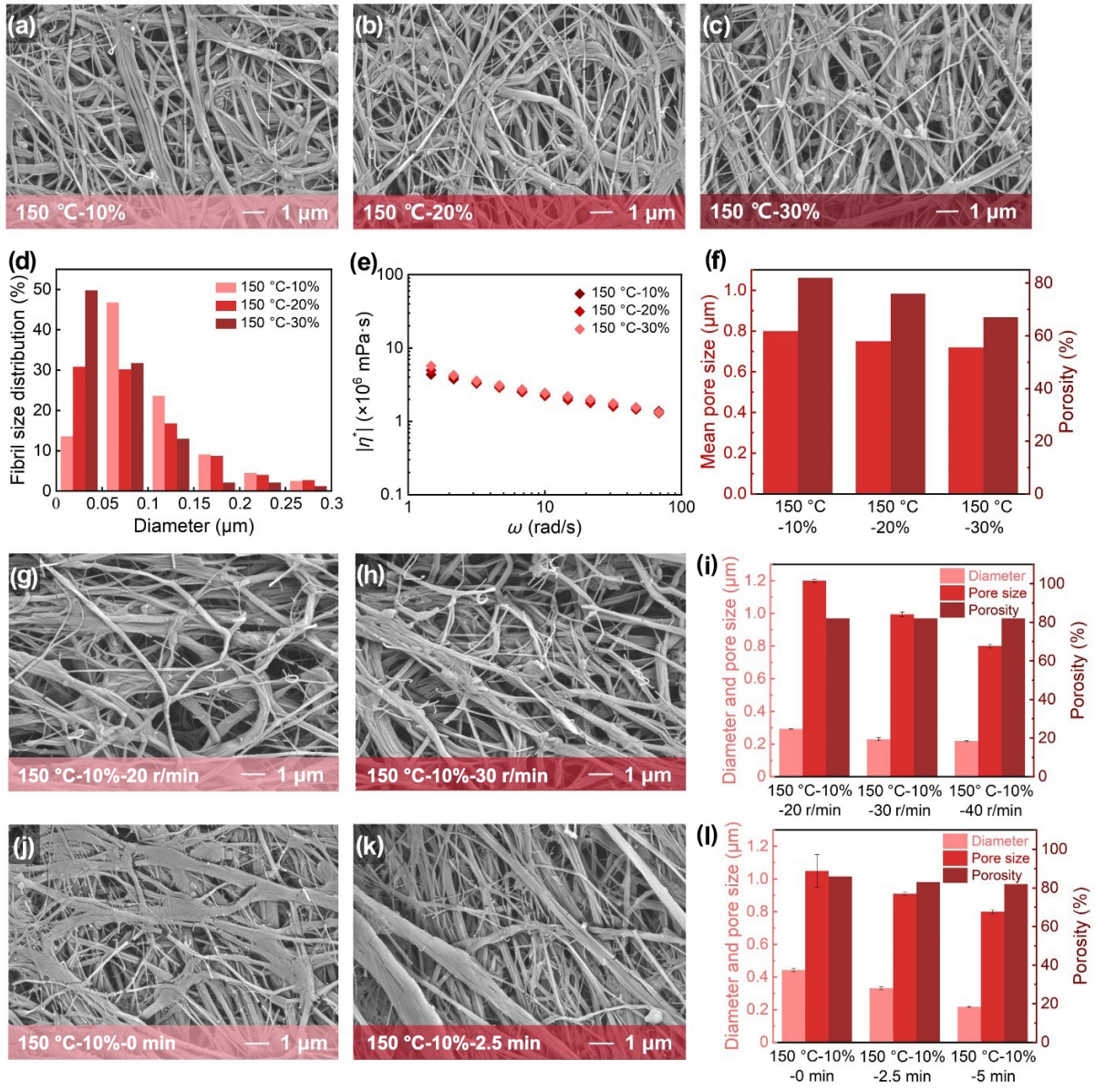

Figure 3 Representative SEM micrographs of PTFE nanofiber membranes prepared at 150 °C with PTFE contents of (a) 10 wt.%, (b) 20 wt.%, and (c) 30 wt.%. (d) Fibril diameter distribution. (e) Frequency-dependent $|\eta^*|$ of PTFE/PCL blends at 150 °C with varying compositions. (f) Average pore size and porosity of PTFE nanofiber membranes. SEM images of membranes prepared at 150 °C with 10 wt.% PTFE at screw speeds of (g) 20 r/min and (h) 30 r/min, with quantitative data of (i) fibril diameter distribution, average pore size, and porosity. SEM images of membranes with 10 wt.% PTFE processed at 150 °C for cycle times of (j) 0 min and (k) 2.5 min, with corresponding quantitative measurements of (l) fibril diameter distribution, average pore size, and porosity.

Notably, despite significant changes in the microstructure, all membranes maintained a high porosity (82%). This indicates that by adjusting the screw speed, allowing effective regulation of the pore size in PTFE nanofiber membranes without sacrificing porosity, providing a critical structural control dimension for meeting different filtration accuracy requirements.

In addition to the instantaneous shear force, the cycle time is also an important factor influencing the PTFE fibrillation process. In this study, the effect of different cycle times (0, 2.5, and 5.0 min) on the PTFE/PCL (10/90 wt.%) blend system and the final membrane structure was investigated at a fixed processing temperature (150 °C) and screw speed (40 r/min). SEM images visually demonstrate the influence of cycle time on the fiber morphology. At 0 min, PTFE crystals had begun to shear into fibers, but the fibers were short and thick, with numerous PTFE aggregates that had not fully dissociated, resulting in a loose fiber network (Fig. 3(j)). As the cycle time increased, the fibrillation of PTFE became more complete, with the fibers becoming longer, more continuous, and the network entanglement significantly improving (Fig. 3(k)). At 5.0 min, PTFE formed a uniform, fine, and highly interconnected three-dimensional nanofiber network, with almost no undissociated particles observed (Fig. 3(a)). Figure 3(l) shows that the average fiber diameter decreases as the cycle time is extended, reducing from 445 nm at 0 min to 217 nm at 5.0 min. The pore size distribution also shifted towards smaller sizes, accompanied by a reduction in the average pore size from 1.05 μm at 0 min to 0.8 μm at 5.0 min. The porosity slightly decreased as the fiber network became denser, from about 86% at 0 min to 82% at 5.0 min. These results indicate that an adequate cycle time is essential for ensuring sufficient PTFE fibrillation, leading to the

formation of fine, uniform nanofiber structures. By controlling the cycle time, the maturity and compactness of the PTFE fiber network can be effectively regulated.

3.2 Membrane structural uniformity and mechanical properties

The excellent processability of PCL at low temperatures allows for effective PTFE fibrillation under milder conditions. The PTFE nanofiber membranes fabricated with PCL as the matrix exhibit a dense and smooth surface (Fig. S2 in the ESM). Moreover, the overall thickness of the membrane can be regulated by varying the initial PTFE/PCL ratio. Figure 4(a) shows the relationship between the nanofiber membrane thickness and PTFE content after the removal of the PCL matrix, which follows a linear trend. Thus, a PTFE nanofiber membrane with a thickness as low as 9 μm can be obtained from a PTFE/PCL composite membrane with an initial PTFE content of 10%. Membrane thickness affects the separation flux of various substances. Additionally, the fiber membranes produced by this method maintain certain mechanical strength, effectively preventing material leakage. Figure 4(b) presents the tensile stress–strain curves of PTFE nanofiber membranes fabricated at various processing temperatures. At the lower processing temperatures of 90 and 120 °C, the higher viscosity of the PCL melt transmits strong shear forces. While this promotes fibrillation, it can also result in uneven fibrillation or the formation of defective fiber structures. These structural imperfections can initiate microcracks at low strains, thereby limiting the enhancement of tensile strength. However, the relatively loose or imperfect network structure provides some space for fiber slippage, resulting in a higher elongation at break compared to the PTFE fiber networks processed at 150 and 180 °C. Notably, at 120 °C, the membrane exhibited an impressively high elongation at break. The fiber network formed at a processing temperature of 150 °C exhibits the optimal entanglement strength. The high entanglement density makes it difficult for fibers to slide and rearrange during stretching; stress is rapidly transferred along the network and concentrated at the entanglement points, resulting in high strength (25.3 MPa), relatively high modulus (56 MPa), and brittle characteristics with low elongation at break. According to the fracture mechanics of fiber networks, when the entanglement strength exceeds the intrinsic strength of the fibers, the fracture mode transitions from fiber debonding to fiber breakage, which is the fundamental reason for the high-strength brittle fracture observed in the 150 °C membrane (Fig. 4(c)). At 180 °C, the PCL melt viscosity decreases,

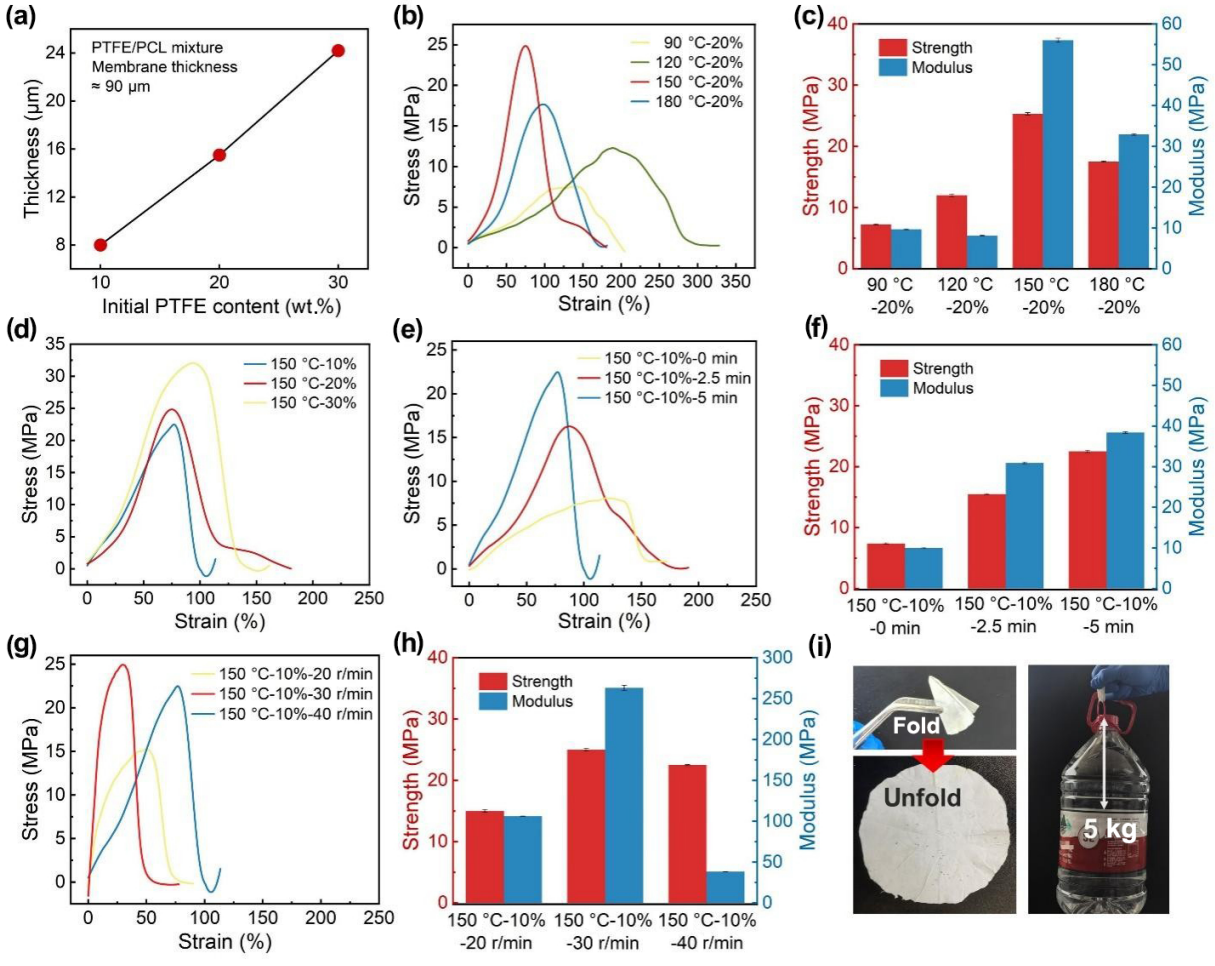

Figure 4 (a) The variation trend of membrane thickness after PCL removal with different initial PTFE contents. (b) Tensile stress–strain curves and (c) corresponding strength–modulus bar chart for membranes processed at 90, 120, 150, and 180 °C (−20%). (d) Stress–strain curves of membrane 150 °C-10%, 150 °C -20%, 150 °C -30%. (e) Stress–strain curves as a function of cycle times. (f) Tensile strength and modulus versus cycle times. (g) Stress–strain curves of PTFE membranes obtained at different screw speeds. (h) Tensile strength and modulus at different screw speeds. (i) Photo of PTFE membrane folded and unfolded, and lightweight PTFE membrane withstands 5 L water weight.

weakening the shear force, which leads to a reduction in the degree of PTFE fibrillation, resulting in thicker fibers and a decrease in the density of entanglement points within the network. During stretching, the fiber network is more prone to slippage and reorganization, and further fibrillation may occur, resulting in a reduction in tensile strength while enhancing the elongation at break.

Under the processing temperature of 150 °C, the tensile strength of the fiber membranes with three different PTFE contents all exceeds 20 MPa. At 30% PTFE content, the tensile strength reaches 31 MPa (Fig. 4(d)). The mechanical characteristics of PTFE nanofiber membranes fabricated at varying cycle times and the evolution of their fiber structure exhibit a strong correlation (Fig. 4(e)). With an increase in cycle time from 0 to 5.0 min, the tensile strength of the membrane monotonically increases from about 9 MPa to approximately 22 MPa. This trend clearly demonstrates that an adequate cycle time is essential to ensure sufficient PTFE fibrillation, leading to the formation of a strong and tough nanofiber network. At 0 min, the insufficiently fibrillated aggregates act as weak points in the network, resulting in low strength. As the cycle time increases, the fibrillation degree deepens, and the number and strength of fiber entanglements increase, which in turn enhances the macroscopic mechanical properties of the membrane. Figure 4(f) shows that the strength and modulus of PTFE nanofiber membranes increase with the extension of cycle time. Mechanical performance of PTFE nanofiber membranes produced under varying screw speeds (Fig. 4(g)) exhibit an intriguing phenomenon: The tensile strength does not change monotonically with screw speed, but reaches its maximum (~ 25 MPa) at 30 r/min, with values of approximately 20 and 22 MPa at 20 and 40 r/min, respectively. Even more impressively, the 150 °C-10% membrane prepared at 30 r/min exhibits an exceptionally high modulus of 273 Mpa (Fig. 4(h)). Such differences are attributed to the distinct fiber network architectures generated under varying shear conditions. A low screw speed (20 r/min) leads to insufficient fibrillation, resulting in coarse fibers, large membrane pores, easy relaxation, and a low retained intrinsic strength of the network structure. In contrast, an excessively high screw speed (40 r/min) subjects the already formed fibers to excessive shear forces, producing finer fibers and slightly weakening either the fiber strength or the junction strength. In comparison, at a moderate screw speed of 30 r/min, an optimal balance is achieved between fiber fineness and membrane pore size, and the relationship between entanglement density and fiber strength is more reasonable, enabling the fiber network to distribute stress most effectively under loading. Although the 150 °C-20% membrane exhibited a low elongation at break, it demonstrated excellent flexibility during bending and folding tests. The ultraflexible nature of this membrane allowed it to be bent and folded into various shapes while recovering to its original form upon unfolding (Fig. 4(i)). Additionally, the lightweight PTFE membrane (density) weighs only 0.2 g and can easily bear a load of 5 L of water without breaking or deforming, further highlighting its excellent mechanical properties.

3.3 Surface properties and oil–water separation of PTFE nanofiber membranes

Figure 5(a) shows the fabricated PTFE nanofiber membranes exhibit oleophilicity, waterproof characteristics, and excellent breathability. First, the PTFE membrane demonstrates favorable air permeability. The rich microporous structure imparts excellent air permeability to the PTFE nanofiber membranes. Figure 5(b) simulates the waterproof breathability of the microporous membrane. When the membrane is placed between air and water environments, a continuous gas flow can pass through the PTFE nanofiber membrane, generating bubbles in the water above. When the membrane is fixed onto the opening of a bottle containing liquid nitrogen and placed in a room-temperature environment, the vapor from the evaporating liquid nitrogen permeates through the PTFE microporous membrane, generating condensed white water vapor.

The surface wettability of membrane materials (particularly their hydrophobicity) is a critical factor that determines their antifouling performance and selectivity in aqueous separation applications. PTFE inherently possesses an extremely low surface energy and is a natural hydrophobic material. However, as shown in this study, the apparent water contact angle (WCA) of PTFE nanofiber membranes prepared via *in situ* fibrillation is significantly affected by the processing temperature, exhibiting a systematic variation. With an increase in processing temperature from 90 to 180 °C, the WCA rises from approximately 105° to 145° (Fig. 5(c)), a trend that aligns with the Cassie–Baxter model [51]. This model suggests that when the membrane surface possesses suitable nanoscale structures, droplets are trapped on the air cushion between these structures, leading to a significant increase in WCA. In this study, processing temperature directly controlled this "air-cushion effect" by altering the fibrillation degree and surface roughness of the PTFE network. At 90 °C, insufficient fibrillation results in a relatively flat fiber network with low surface roughness, causing greater contact between water droplets and the solid surface, thus leading to a lower WCA (~ 105°). As the temperature increases, fibrillation improves, surface roughness increases, and the WCA gradually rises to around 140°. At 180 °C, although the average fiber diameter increases, the fiber network likely forms a more complex, multi-scale loose structure, further enhancing surface roughness and the air-trapping effect, resulting in a WCA approaching that of superhydrophobic surfaces (~ 145°). The findings demonstrate that by regulating the processing temperature, the wettability of PTFE nanofiber membranes can be effectively tuned from hydrophobic to near-superhydrophobic. Membranes with higher WCAs (e.g., 180 °C-20%) exhibit stronger resistance to water infiltration and fouling when exposed to aqueous solutions or emulsions, which is crucial for extending membrane lifespan in harsh water environments.

In contrast, PTFE nanofiber membranes exhibit superoleophilic properties. As shown in the optical image in Fig. 5(d), when an oil droplet (chloroform, red) is placed on the PTFE membrane surface, the droplet is rapidly and completely absorbed into the fiber pores, resulting in an oil contact angle close to 0°, demonstrating the exceptional oil-absorbing capability of the PTFE nanofiber membrane. However, deionized water droplets exhibit a relatively large contact angle on the membrane surface. The distinct variance in wettability between water (methylene blue) and oil on the PTFE nanofiber membrane enables efficient oil–water separation. The oil–water separation performance was assessed using a Buchner funnel equipped with a custom-designed apparatus (Fig. 5(e)). The PTFE nanofiber membrane was clamped between two glass filtration cylinders and a conical flask, sealed with a clamp. A 1:1 (v/v) mixture of chloroform (red) and deionized water (blue) was poured into the upper glass tube, and phase separation proceeded

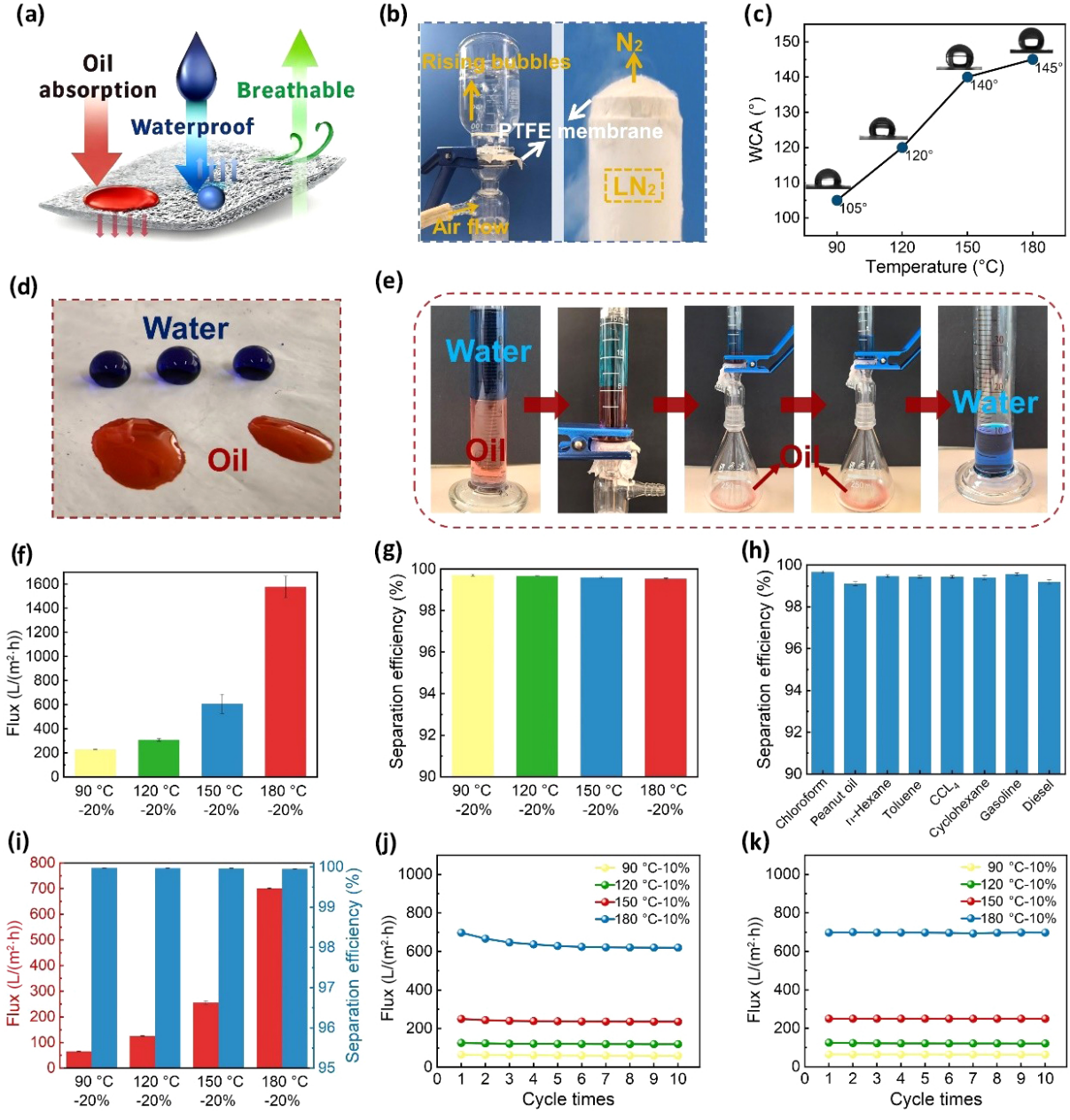

Figure 5 (a) Schematic illustration of the PTFE membrane functions: breathability, waterproofing, and oleophilicity. (b) Example demonstration of air permeability. (c) Water contact angles of PTFE nanofiber membranes prepared at different processing temperatures. (d) Example demonstration of hydrophobic and oleophilic behaviors. (e) Schematic illustration of the apparatus and separation procedure for separating a trichloromethane–water mixture (volume ratio 1:1) using a PTFE nanofiber membrane. (f) Filtration fluxes of four membranes (90 °C-10%, 120 °C-10%, 150 °C-10%, and 180 °C-10%) and their (g) separation efficiencies. (h) Separation efficiencies for various oil–water mixtures using the 180 °C-10% membrane. (i) Filtration fluxes and Separation efficiencies for emulsion filtration using the four membranes (90 °C-10%, 120 °C-10%, 150 °C-10%, and 180 °C-10%). (j) Changes in flux during 10 consecutive cycles of continuous separation of a trichloromethane/water emulsion. (k) Flux variations observed after cleaning the membrane following each cycle during the 10-cycle continuous separation of the trichloromethane/water emulsion (i.e., flux recovery after each washing step).

under gravitational force. Due to the oleophilic nature and high porosity of the PTFE nanofiber membrane, oil droplets passed through the membrane and entered the conical flask below, while PTFE's superhydrophobicity and ultrafine pore size retained the deionized water in the upper glass tube. The separation performance of four different membranes (90 °C-10%, 120 °C-10%, 150 °C-10%, and 180 °C-10%) was examined, as shown in Fig. 5(f). It is evident that the oil flux increases exponentially with processing temperature, which originates from the growth in pore size under high-temperature processing conditions. At 180 °C, the flux reaches 1578.9 L/(m²·h). Furthermore, the separation efficiency of PTFE nanofiber membranes at all processing temperatures exceeds 99.5% (Fig. 5(g)). To investigate the separation behavior of PTFE nanofiber membranes toward oils with varying viscosities and densities, the 180 °C-10% PTFE nanofiber membrane was further subjected to oil–water separation tests with cyclohexane, diesel, and edible soybean oil. The results showed that the PTFE membrane achieved separation efficiencies exceeding 99% for all tested oil droplets, demonstrating that PTFE nanofiber membranes are highly effective for a wide range of oil–water mixtures (Fig. 5(h)).

Oil–water emulsion separation was further simulated in this study. In practical scenarios, oil–water systems are frequently present as emulsions, and the ability to efficiently separate such emulsions is crucial for industrial processing and wastewater treatment. The PTFE nanofiber membrane exhibits excellent capability for separating water-in-oil emulsions. Using the same Buchner-funnel setup, a separation experiment was carried out using a chloroform/water emulsion stabilized with surfactants. The results show that all four membranes achieved extremely high separation efficiencies of up to 99.99%. Figure S3 in the ESM shows the appearance of the oil-in-water emulsion prior to and following separation. In addition, membranes with larger pore sizes exhibited higher permeation flux. As shown in Fig. 5(i), the chloroform fluxes of the membranes prepared at 90 °C-10%, 120 °C-10%, 150 °C-10%, and 180 °C-10% were 65.6, 125.6, 255.9, and 700.62 L/(m^2·h), respectively. Moreover, the durability and reusability of the membrane was evaluated by recording the permeation flux over 10 continuous separation cycles using the same membrane sample. The membrane prepared at 180 °C, which possesses a relatively large pore size, exhibited a pronounced decrease in flux during the 10 cycles, whereas the flux decline for membranes with smaller pore sizes was minimal (Fig. 5(j)). Fortunately, the initial flux of all membranes could be restored after simple rinsing following each separation cycle. Even after 10 cycles, the separation efficiency remained comparable to the initial performance. Therefore, PTFE nanofiber membranes demonstrate excellent reusability (Fig. 5(k)).

3.4 High-precision solid–liquid filtration performance

Solid–liquid filtration constitutes a key focus of this study. For high-precision separation, microporous membranes must possess strong resistance to acidic and alkaline corrosion and robust mechanical stability in order to operate reliably under harsh environments and high pressures. All PTFE nanofiber membranes inherit the intrinsic chemical inertness of PTFE. After immersion in 98% H_2SO_4 and 40% NaOH for 30 min, no visible changes were observed in either the membrane appearance or microstructure (Fig. 6(a)), demonstrating their suitability for long-term filtration under aggressive chemical conditions. To systematically evaluate the filtration accuracy and efficiency of PTFE membranes with different structures, we employed submicron SiO_2 microspheres, CNTs, and

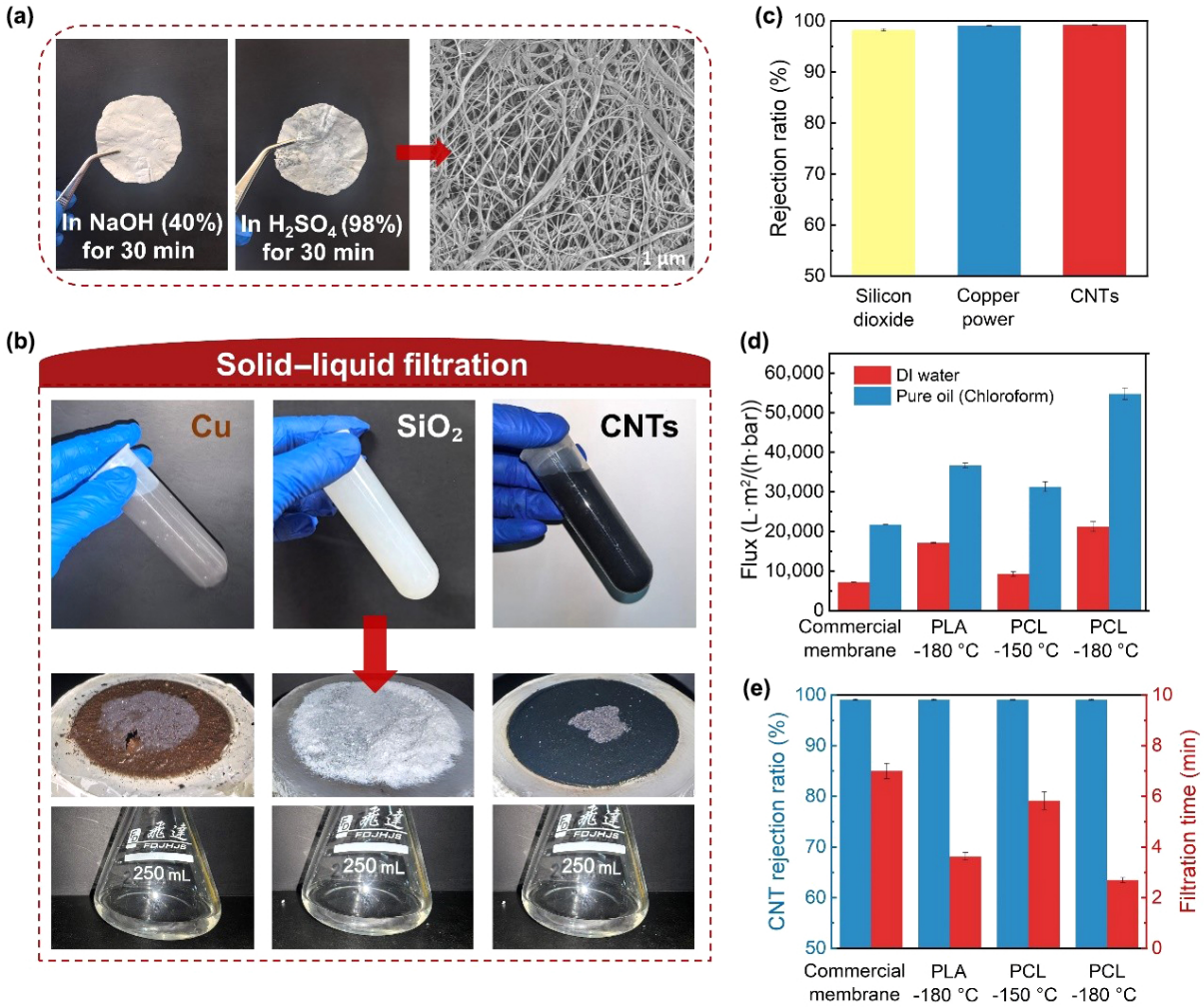

Figure 6 (a) Optical photographs and SEM images of PTFE nanofiber membranes after immersion in strong acid and strong alkali solutions for 30 min. (b) Schematic illustration of the solid–liquid separation process for three types of solids (copper powder, silica powder, and carbon nanotubes). (c) Average separation efficiencies of different types of PTFE nanofiber membranes. (d) Comparison of deionized water flux and pure oil flux among a commercial membrane, a PTFE/PLA-180 °C membrane, a PTFE/PCL-150 °C membrane, and a PTFE/PCL-180°C membrane. (e) Comparison of CNT rejection ratio and filtration time for the four membranes (commercial membrane, PTFE/PLA-180 °C membrane, PTFE/PCL-150 °C membrane, and PTFE/PCL-180 °C membrane) (an effective membrane area of 12.56 cm^2, and repeated three times).

micron-sized copper powders as challenge particles. As shown in Fig. 6(b), the suspensions before and after filtration display a clear contrast: The filtrates are optically transparent in all cases. Figure 6(c) shows the retention rates for the three types of challenge particles using membranes fabricated at 180 °C, highlighting the excellent physical sieving capability of the PTFE nanofiber membranes. For submicron SiO_2 particles, the PTFE/PCL-180 °C-10% membrane exhibits a slightly lower retention rate (98.5%) due to the presence of some pores comparable to or larger than the particle size. Nevertheless, the membrane still demonstrates impressive separation performance. This is attributed to the significantly smaller fiber diameter produced in the PTFE/PCL system, which results in a higher surface-area-to-volume ratio. Under identical conditions, finer fibers exhibit a higher single-fiber collection efficiency. Moreover, diffusion plays a dominant role in the capture of small particles; finer fibers reduce inter-fiber spacing, increasing the probability of particle interception during Brownian motion [52]. Consequently, the PTFE/PCL membrane outperforms the PTFE/PLA counterpart in ultrafine particulate filtration. For the separation of micron-sized Cu particles, the PTFE/PCL-180 °C membrane—with its open micron-scale pore structure—achieves > 99% retention for Cu powders in the 1–5 μm range. We further investigated solid–liquid separation performance using CNTs as representative nanoscale particles. Before filtration tests, the pure water flux and pure oil (chloroform) flux of PTFE/PCL-150 °C-10% and PTFE/PCL-180 °C-10% membranes were measured under vacuum filtration. Ethanol pre-wetting was applied to facilitate wetting and solvent permeation. For comparison, we additionally prepared PTFE/PLA-180 °C-10% nanofiber membranes, which had similar mechanical properties to PTFE/PCL-150 °C-10% membranes and treated under the same conditions as PTFE/PLA-180 °C-10% membranes, and we evaluated a commercial PTFE stretched membrane (Shanghai Xingya Purification Materials Co., Ltd. , which has a thickness of 65–100 μm, a pore size of 80 μm) under identical test conditions. The results reveal that all three PTFE nanofiber membranes produced via *in-situ* fibrillation exhibit significantly higher water and oil fluxes compared to the commercial stretched membrane. Notably, the PTFE/PCL-180 °C-10% membrane shows a pure water flux of 21,235 L/(m^2·h) and a pure oil flux of 54,760 L/(m^2·h), which are approximately three and four times those of the commercial membrane, and 1.3 and 1.5 times those of the PTFE/PLA-180 °C-10% membrane, respectively (Fig. 6(d)). To further demonstrate solid–liquid separation capability, CNTs were treated with H_2SO_4 to achieve carboxylated CNT dispersions. The dispersions were filtered using the four types of membranes, and all membranes achieved > 99% retention. Despite similar retention efficiencies, the PTFE/PCL-180 °C-10% membrane exhibited the shortest filtration time, outperforming the PTFE/PLA-180 °C-10% membrane and showing markedly higher filtration efficiency than the commercial stretched membrane (Fig. 6(e)).

4 Conclusions

In this work, PCL was used as a removable matrix, and its broad processing temperature window from 90 to 180 °C enabled the fabrication of PTFE nanofiber membranes via an *in-situ* shear-induced fibrillation method. This approach establishes a highly controllable process for producing PTFE nanofiber membranes. By precisely tuning the processing temperature, screw speed, and cycle time, the fiber diameter and pore-size distribution can be finely adjusted over a wide range, enabling the "targeted design" of membrane properties. The resulting PTFE nanofiber membranes exhibit high mechanical strength (25.3 MPa), excellent chemical stability, and tunable surface wettability ranging from hydrophobic to near-superhydrophobic (WCA ~ 145°). Their intrinsic super-oleophilicity and high porosity enable efficient gravity-driven oil–water separation and surfactant-stabilized emulsion separation, achieving > 99.9% separation efficiency with high flux and good recyclability. Furthermore, the membranes show outstanding high-precision solid–liquid filtration performance. They effectively capture submicron SiO_2 particles, micron-sized Cu powders, and carbon nanotubes with > 99% rejection, while delivering water and oil fluxes several times higher than commercial stretched PTFE membranes. Overall, this study presents a scalable and structurally tunable strategy for producing PTFE nanofiber membranes with superior mechanical integrity, chemical resistance, and exceptional separation capabilities, highlighting their strong potential for advanced oil–water separation and high-precision solid–liquid filtration applications.

Electronic Supplementary Material: Supplementary material (additional DSC images, optical images of the PTFE nanofiber membrane, comparative images of the water-in-oil emulsion before and after separation, quantitative analysis formulas for viscosity, and statistical tables of relevant fiber membrane structure data) is available in the online version of this article at https://doi.org/10.26599/NR.2026.94908740.

Data availability

All data needed to support the conclusions in the paper are presented in the manuscript and the Electronic Supplementary Material. Additional data related to this paper may be requested from the corresponding author upon request.

Acknowledgment

This study received financial support from National Natural Science Foundation of China (No. 52175341), Shandong Provincial Natural Science Foundation (No. ZR2022JQ24), Funding Project of Jinan City's New Twenty Items for Colleges and Universities (No. 202333038), Excellent Young Team Project of Central Universities (No. 2023QNTD002), and Qingdao Key Technology Research and Industrialization Demonstration Project (No. 24-1-2-qljh-10-gx).

Declaration of competing interest

All the contributing authors report no conflict of interests in this work.

Author contribution statement

Z. L. W.: Data curation, formal analysis, methodology, validation, writing – original draft. G. L. W.: Conceptualization, project administration, resources, writing – original draft, experimental design, funding acquisition. J. L. C.: Writing – review & editing, supervision. R. Z. S.: Writing – review & editing, conceptualization. G. Q. Z.: Project administration, validation, funding acquisition. All the authors have approved the final manuscript.

Use of AI statement

None.

References

[1] Lee, G.; Lee, K.; Sun, S.; Song, T.; Paik, U. Engineering SiO_2 nanoparticles: A perspective on chemical mechanical planarization slurry for advanced semiconductor processing. *Kona Powder Part. J.* **2025**, *42*, 79–99.

[2] Wang, Y. C.; Zhang, Y.; Liang, L.; Tu, F.; Li, Z. J.; Tang, X. J.; Dai, L.; Li, L. L. Research progress on membrane separation technology for oily wastewater treatment. *Toxics* **2024**, *12*, 794.

[3] Li, M.; Jia, X.; Wang, L.; Gao, G. Y.; Feng, X. F.; Li, C. Y. Research on modified carbon nanotubes in wastewater treatment. *Catalysts* **2022**, *12*, 1103.

[4] Kato, S.; Kansha, Y. Comprehensive review of industrial wastewater treatment techniques. *Environ. Sci. Pollut. Res.* **2024**, *31*, 51064–51097.

[5] Eggimann, S.; Truffer, B.; Feldmann, U.; Maurer, M. Screening European market potentials for small modular wastewater treatment systems-an inroad to sustainability transitions in urban water management. *Land Use Policy* **2018**, *78*, 711–725.

[6] Kiss, A. A.; Smith, R. Rethinking energy use in distillation processes for a more sustainable chemical industry. *Energy* **2020**, *203*, 117788.

[7] Farid, M. U.; Kharraz, J. A.; Sun, J. W.; Boey, M. W.; Riaz, M. A.; Wong, P. W.; Jia, M. Y.; Zhang, X. N.; Deka, B. J.; Khanzada, N. K. et al. Advancements in nanoenabled membrane distillation for a sustainable water-energy-environment nexus. *Adv. Mater.* **2024**, *36*, 2307950.

[8] Guerrini, L.; Luca Pantani, O.; Parenti, A. The impact of vertical centrifugation on olive oil quality. *J. Food Process Eng.* **2017**, *40*, e12489.

[9] Zulbeari, N.; Lund, N. E.; Holm, R. Small-scale aqueous suspension preparation using dual centrifugation: The effect of process parameters on the sizes of drug particles. *Eur. J. Pharm. Sci.* **2025**, *205*, 106980.

[10] Antonopoulou, E.; Rohmann-Shaw, C. F.; Sykes, T. C.; Cayre, O. J.; Hunter, T. N.; Jimack, P. K. Numerical and experimental analysis of the sedimentation of spherical colloidal suspensions under centrifugal force. *Phys. Fluids* **2018**, *30*, 030702.

[11] Tehrani, S. F.; Bharadwaj, P.; Leblond Chain, J.; Roullin, V. G. Purification processes of polymeric nanoparticles: How to improve their clinical translation. *J. Control. Release* **2023**, *360*, 591–612.

[12] Zeng, G. S.; Zhu, Y. G.; Chen, W. A brief review of micro-particle slurry rheological behavior in grinding and flotation for enhancing fine mineral processing efficiency. *Minerals* **2023**, *13*, 792.

[13] Ren, L. Y. Editorial for special issue "advances on fine particles and bubbles flotation". *Minerals* **2024**, *14*, 439.

[14] Soliman, M. G.; Martinez-Serra, A.; Dobricic, M.; Trinh, D. N.; Cheeseman, J.; Spencer, D. I. R.; Monopoli, M. P. Protocols for isolation and characterization of nanoparticle biomolecular corona complexes. *Front. Toxicol.* **2024**, *6*, 1393330.

[15] Wang, X.; Cheng, W. L.; Wang, D.; Ni, X. H.; Han, G. P. Electrospun polyvinylidene fluoride-based fibrous nanocomposite membranes reinforced by cellulose nanocrystals for efficient separation of water-in-oil emulsions. *J. Membrane Sci.* **2019**, *575*, 71–79.

[16] Cheng, X. Q.; Jiao, Y.; Sun, Z. K.; Yang, X. B.; Cheng, Z. J.; Bai, Q.; Zhang, Y. J.; Wang, K.; Shao, L. Constructing scalable superhydrophobic membranes for ultrafast water–oil separation. *ACS Nano* **2021**, *15*, 3500–3508.

[17] Jiang, J. K.; Wan, S. D.; Wen, C.; Tang, L.; Xu, N. Frontiers in innovative materials and technologies for oil–water separation. *Polymers* **2025**, *17*, 1635.

[18] José, M. H.; Canejo, J. P.; Godinho, M. H. Oil/water mixtures and emulsions separation methods—An overview. *Materials* **2023**, *16*, 2503.

[19] Liao, Y.; Loh, C. H.; Tian, M.; Wang, R.; Fane, A. G. Progress in electrospun polymeric nanofibrous membranes for water treatment: Fabrication, modification and applications. *Prog. Polym. Sci.* **2018**, *77*, 69–94.

[20] Chen, W. M.; Gu, Z. P.; Ran, G.; Li, Q. B. Application of membrane separation technology in the treatment of leachate in China: A review. *Waste Manage.* **2021**, *121*, 127–140.

[21] Azmi, L. S.; Jabit, N. 'A.; Ismail, S.; Ku Ishak, K. E. H.; Abdullah, T. K. Membrane filtration technologies for sustainable industrial wastewater treatment: A review of heavy metal removal. *Desalin. Water Treat.* **2025**, *323*, 101321.

[22] Ge, J. L.; Zong, D. D.; Jin, Q.; Yu, J. Y.; Ding, B. Biomimetic and superwettable nanofibrous skins for highly efficient separation of oil-in-water emulsions. *Adv. Funct. Mater.* **2018**, *28*, 1705051.

[23] Li, B. F.; Qi, B.; Guo, Z. Y.; Wang, D. X.; Jiao, T. F. Recent developments in the application of membrane separation technology and its challenges in oil-water separation: A review. *Chemosphere* **2023**, *327*, 138528.

[24] Tan, C. J.; Wu, S. Y.; Weng, M. N.; Xian, J. L.; Chen, Z. X.; Qi, Y. T.; Zhang, J. T.; Chen, J.; Bo, H. B. Explore the application potential of nanoporous material-based membrane separation technology in the energy sector. *J. Environ. Chem. Eng.* **2025**, *13*, 120322.

[25] Ji, K. Y.; Liu, C. K.; He, H. J.; Mao, X.; Wei, L.; Wang, H.; Zhang, M. D.; Shen, Y. T.; Sun, R. J.; Zhou, F. L. Research progress of water treatment technology based on nanofiber membranes. *Polymers* **2023**, *15*, 741.

[26] Yan, X. H.; Xiao, X.; Au, C.; Mathur, S.; Huang, L. J.; Wang, Y. X.; Zhang, Z. J.; Zhu, Z. J.; Kipper, M. J.; Tang, J. G. et al. Electrospinning nanofibers and nanomembranes for oil/water separation. *J. Mater. Chem. A* **2021**, *9*, 21659–21684.

[27] Li, J. J.; Zhu, L. T.; Luo, Z. H. Electrospun fibrous membrane with enhanced swithchable oil/water wettability for oily water separation. *Chem. Eng. J.* **2016**, *287*, 474–481.

[28] Han, J. C.; Xie, N.; Ju, J. G.; Zhang, Y.; Wang, Y. C.; Kang, W. M. Developments of electrospinning technology in membrane bioreactor: A review. *Chemosphere* **2024**, *364*, 143091.

[29] Ahmed, F. E.; Lalia, B. S.; Hashaikeh, R. A review on electrospinning for membrane fabrication: Challenges and applications. *Desalination* **2015**, *356*, 15–30.

[30] T M, S.; Arshad, A. B.; Lin, P. T.; Widakdo, J.; H K, M.; Austria, H. F. M.; Hu, C. C.; Lai, J. Y.; Hung, W. S. A review of recent progress in polymeric electrospun nanofiber membranes in addressing safe water global issues. *RSC Adv.* **2021**, *11*, 9638–9663.

[31] Wu, J. R.; He, J.; Yin, K.; Zhu, Z.; Xiao, S.; Wu, Z. P.; Duan, J. A. Robust hierarchical porous PTFE film fabricated via femtosecond laser for self-cleaning passive cooling. *Nano Lett.* **2021**, *21*, 4209–4216.

[32] Wu, Z. C.; Hao, X. T.; Wu, M. Y.; Wu, Q. Y.; Yang, J. J.; Liu, J. Y.; Zhang, J. N. Superhydrophilic modification of polytetrafluoroethylene (PTFE) hollow fiber membrane by a novel miniemulsion template method. *J. Membrane Sci.* **2025**, *722*, 123920.

[33] Yu, Y. F.; Zhang, L.; Li, X. D.; Ye, J. L.; Meng, J. Q. Multifunctionalization of PTFE membrane surface for biofouling resistance and oil/water separation performance improvement. *J. Environ. Chem. Eng.* **2023**, *11*, 109158.

[34] Cui, Z. L.; Drioli, E.; Lee, Y. M. Recent progress in fluoropolymers for membranes. *Prog. Polym. Sci.* **2014**, *39*, 164–198.

[35] Li, K. L.; Zhang, Y.; Xu, L. L.; Zeng, F. F.; Hou, D. Y.; Wang, J. Optimizing stretching conditions in fabrication of PTFE hollow fiber

membrane for performance improvement in membrane distillation. *J. Membrane Sci.* **2018**, *550*, 126–135.
[36] Jia, J. X.; Kang, G. D.; Cao, Y. M. Effect of stretching parameters on structure and properties of polytetrafluoroethylene hollow-fiber membranes. *Chem. Eng. Technol.* **2016**, *39*, 935–944.
[37] Ranjbarzadeh-Dibazar, A.; Shokrollahi, P.; Barzin, J.; Rahimi, A. Lubricant facilitated thermo-mechanical stretching of PTFE and morphology of the resulting membranes. *J. Membrane Sci.* **2014**, *470*, 458–469.
[38] Zhang, Y. Y.; Ge, Q.; Yang, L. L.; Shi, X. J.; Li, J. J.; Yang, D. Q.; Sacher, E. Durable superhydrophobic PTFE films through the introduction of micro- and nanostructured pores. *Appl. Surf. Sci.* **2015**, *339*, 151–157.
[39] Zhao, P. F.; Soin, N.; Prashanthi, K.; Chen, J. K.; Dong, S. R.; Zhou, E. P.; Zhu, Z. G.; Narasimulu, A. A.; Montemagno, C. D.; Yu, L. Y. et al. Emulsion electrospinning of polytetrafluoroethylene (PTFE) nanofibrous membranes for high-performance triboelectric nanogenerators. *ACS Appl. Mater. Interfaces* **2018**, *10*, 5880–5891.
[40] Pang, H. L.; Tian, K. X.; Li, Y. P.; Su, C. L.; Duan, F.; Xu, Y. Super-hydrophobic PTFE hollow fiber membrane fabricated by electrospinning of Pullulan/PTFE emulsion for membrane deamination. *Sep. Purif. Technol.* **2021**, *274*, 118186.
[41] Qin, Z. L.; Xiang, H. Q.; Liu, J. G.; Zeng, X. Y. High-performance oil-water separation polytetrafluoroethylene membranes prepared by picosecond laser direct ablation and drilling. *Mater. Design* **2019**, *184*, 108200.
[42] Kacem, E.; Suk, H. D.; Ponnamma, D.; Hassan, M. K.; Hawari, A.; Alshammari, B. A.; Al‐Ejji, M. Exploring 3D printing and electrospinning technologies for advanced porous membrane fabrication: A review. *Adv. Mater. Technol.* **2025**, *10*, 70032.
[43] Yang, J. Y.; Su, R.; Ying, H. M.; Hu, L.; Ruan, X. D. Preparation and characterization of complex shaped polytetrafluoroethylene (PTFE) parts based on vat photopolymerization 3D printing. *Mater. Today Commun.* **2023**, *36*, 106764.
[44] Chai, J. L.; Wang, G. L.; Zhang, A. M.; Li, X. Y.; Xu, Z. R.; Zhao, J. C.; Zhao, G. Q. Robust polytetrafluoroethylene (PTFE) nanofibrous membrane achieved by shear-induced *in-situ* fibrillation for fast oil/water separation and solid removal in harsh solvents. *Chem. Eng. J.* **2023**, *461*, 141971.
[45] Shao, R. Z.; Wang, G. L.; Chai, J. L.; Wang, G. Z.; Zhao, G. Q. Flexible, reliable, and lightweight multiwalled carbon nanotube/polytetrafluoroethylene membranes with dual-nanofibrous structure for outstanding EMI shielding and multifunctional applications. *Small* **2024**, *20*, 2308992.
[46] Zhou, T.; Yao, Y. Y.; Xiang, R. L.; Wu, Y. R. Formation and characterization of polytetrafluoroethylene nanofiber membranes for vacuum membrane distillation. *J. Membrane Sci.* **2014**, *453*, 402–408.
[47] Shi, Y. D.; Hu, Y.; Shen, J. B.; Guo, S. Y. Optimized microporous structure of ePTFE membranes by controlling the particle size of PTFE fine powders for achieving high oil–water separation performances. *J. Membrane Sci.* **2021**, *629*, 119294.
[48] Chai, J. L.; Wang, G. L.; Zhang, A. M.; Li, S.; Zhao, J. C.; Zhao, G. Q.; Park, C. B. Ultra-ductile and strong *in-situ* fibrillated PLA/PTFE nanocomposites with outstanding heat resistance derived by CO_2 treatment. *Compos. Part A: Appl. Sci. Manuf.* **2022**, *155*, 106849.
[49] Hohman, M. M.; Shin, M.; Rutledge, G.; Brenner, M. P. Electrospinning and electrically forced jets. I. Stability theory . *Phys. Fluids* **2001**, *13*, 2201–2220.
[50] Hohman, M. M.; Shin, M.; Rutledge, G.; Brenner, M. P. Electrospinning and electrically forced jets. II. Applications.*Phys. Fluids* **2001**, *13*, 2221–2236.
[51] Liu, T. L.; Chen, Z. Y.; Kim, C. J. A dynamic Cassie-Baxter model. *Soft Matter* **2015**, *11*, 1589–1596.
[52] Kim, H. B.; Lee, W. J.; Choi, S. C.; Lee, K. B.; Lee, M. H. Filter quality factors of fibrous filters with different fiber diameter. *Aerosol Sci. Technol.* **2021**, *55*, 154–166.